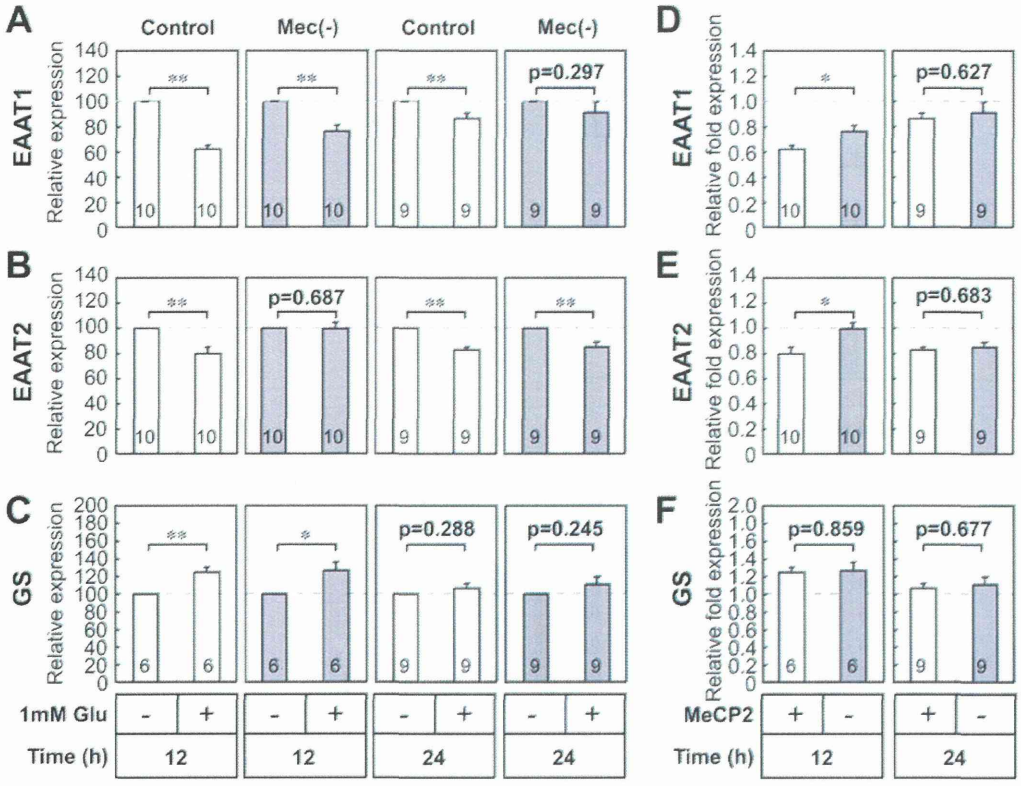

Figure 3. Effect of glutamate on glutamine synthetase and glutamate transporter gene expression in MeCP2-null astrocytes. A–C. Effects of Glu on Glu clearance-related genes in wild-type (white column) and MeCP2-null (gray column) astrocytes. Semi-quantitative RT-PCR analysis of Glu clearance-related genes, EAAT1 (**A**), EAAT2 (**B**), and GS (**C**), was performed in the control and MeCP2-null astrocytes 12 or 24 h after treatment with 1.0 mM Glu. The bands corresponding to PCR products were quantified by densitometry, normalized against HPRT levels, and expressed as % of controls (equals 100%). Bars represent the means ± SE of samples from 3–4 independent experiments (*p<0.05, **p<0.01). **D–F.** Comparison of the effects of Glu on EAAT1, EAAT2 or GS expression in the control and MeCP2-null astrocytes. The ratio of EAAT1/HPRT (**D**), EAAT2/HPRT (**E**) or GS/HPRT (**F**) in each treatment group was normalized against that of the non-treated astrocytes from each group. Bars represent the means ± SE of samples from 3–5 independent experiments (*p<0.05). Numbers in each column indicate the total number of samples analyzed.
doi:10.1371/journal.pone.0035354.g003

overexpression of MeCP2 inhibited the differentiation of neuroepithelial cells into GFAP-positive glial cells [34]. Our recent study in RTT-model ES cells also demonstrated that MeCP2 is involved in gliogenesis during neural differentiation via inhibition of GFAP expression [12]. Therefore, MeCP2 may be involved not only in the suppression of astroglial genes in neuroepithelial cells/neurons during neurogenesis, but also in the physiological regulation of astroglial gene expression in astrocytes.

We also demonstrated that MeCP2 is not essential for cell growth or cell viability in in vitro models of astrocyte injury, such as H_2O_2 oxidative stress and ammonia neurotoxicity. On the other hand, it has been reported that MeCP2 is involved in regulating astrocyte proliferation, and are probably due to distinct differences in culture conditions, specifically the presence of serum [10]. Consistent with these results, obvious neuronal and glial degeneration had not been observed in RTT [6,35]. These observations suggest that RTT is not caused by reduced cell numbers, but rather by dysfunction of specific cell types in the brain.

The regulation of Glu levels in the brain is an important component of plasticity at glutamatergic synapses, and of neuronal damage via excessive activation of Glu receptors [15,16]. Astrocytic uptake of Glu, followed by conversion of Glu to Glutamine (Gln), is the predominant mechanism of inactivation of Glu once it has been released in the synaptic cleft. This uptake involves two transporters, EAAT1/GLAST and EAAT2/GLT-1 [16]. Increases in extracellular Glu, present in many brain injuries, are sufficient to modulate the expression of Glu transporters and GS [16,29]. Furthermore, application of 0.5–1.0 mM Glu to cultured cortical astrocytes causes a decline in EAAT1/GLAST and EAAT2/GLT-1 expression [29]. Our present studies reveal that 1.0 mM extracellular Glu is sufficient to inhibit astroglial Glu transporter expression and to stimulate GS expression in control astrocytes. However, such regulatory influences on Glu transporters are impaired by MeCP2 deficiency. Therefore, MeCP2 may regulate the expression of Glu transporters under physiological conditions. Currently, little is known about the promoter regions of the main Glu transporters [36,37]. Promoter analysis in each gene may help to elucidate the complex regulations of astroglial genes by MeCP2.

On the other hand, in our culture conditions, MeCP2 deficiency did not impair the expression of GS transcripts in cultured astrocytes, but did affect the expression of GS protein. A very recent study has shown that defects in the AKT/mTOR pathway

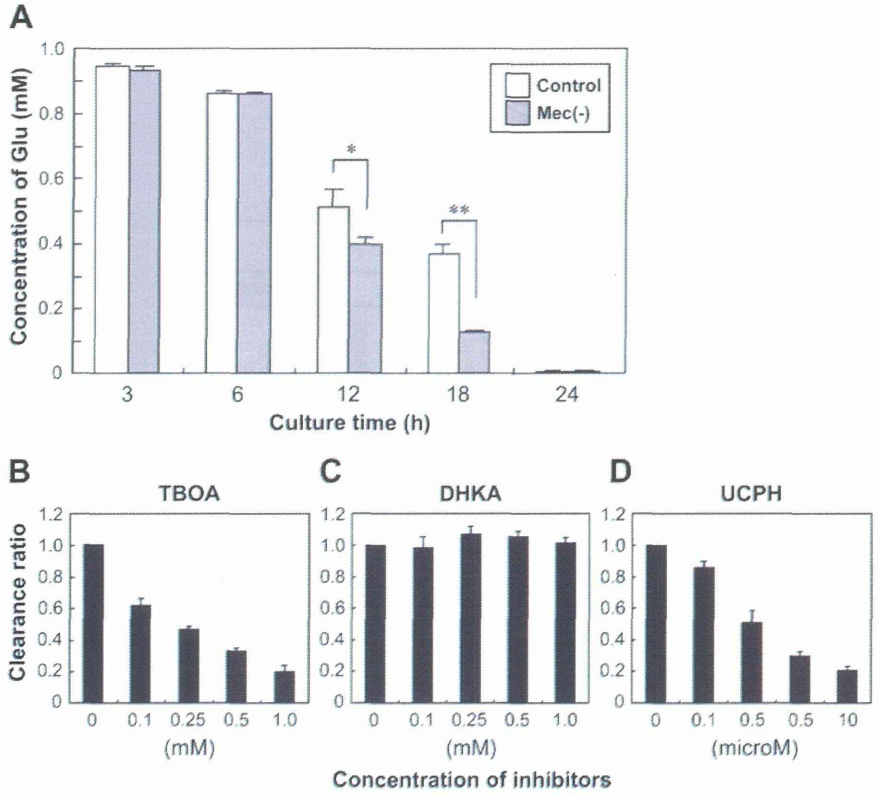

Figure 4. Comparison of glutamate clearance in wild-type and MeCP2-null astrocytes. A. Time-dependent reduction of extracelluar Glu concentration in wild-type (white column) and MeCP2-null (gray column) astrocyte cultures. After treatment with 1.0 mM Glu, culture supernatant was collected at the indicated times for the determination of Glu concentration. The graph shows the concentration of Glu in control and MeCP2-null astrocyte culture medium. Bars represent the means ± SE of samples from three independent experiments (*$p<0.05$). **B–D.** Effects of inhibitors of glutamate transporters (**B,** TBOA; **C,** DHKA; **D,** UCPH) on Glu clearance. Astrocytes were exposed to the indicated concentration of Glu transporter inhibitors, and then 0.1 mM Glu was added; culture supernatant was collected for the determination of Glu concentration at 2 h. The graphs show the clearance ratio upon treatment with each inhibitor. The clearance ratio in the indicated concentration groups was expressed by defining the control level (no inhibitor) as 1.0. Bars represent the means ± SE of samples from three independent experiments.
doi:10.1371/journal.pone.0035354.g004

are responsible for altered translational control in MeCP2 mutant neuron [38]. These findings suggest that a deficit in protein synthesis and/or turnover in the MeCP2-null astrocytes might influence the final levels of GS protein. Further studies are necessary to investigate whether MeCP2 deficiency impairs the synthesis and turnover of proteins in RTT.

The most important finding in this study was that MeCP2 deficiency in astrocytes accelerates Glu clearance. Consistent with this, RTT is associated with abnormalities in the Glu metabolism [24]. Some studies have demonstrated increases in Glu levels in the cerebrospinal fluid (CSF) of human RTT patients [18,19]. On the other hand, in animal studies there have been instances of decreased Glu levels and/or Glu/Gln ratios, as determined by in MR spectroscopy [8,21,22,23]. Furthermore, MeCP2-deficient microglia release an abnormally high level of Glu, causing excitotoxicity that may contribute to dendritic and synaptic abnormalities in RTT [11]. These results clearly suggest that MeCP2 has the potential to regulate Glu levels in the brain under certain circumstances. Glu levels are altered in the RTT brain, but the mechanisms responsible for the changes in Glu metabolism are unknown. In light of our findings, we speculate that abnormal expression of Glu transporters and GS resulting from MeCP2 deficiency could lead to abnormal Glu clearance in astrocytes and in turn to altered levels of Glu in RTT brain. Additional studies are needed to determine the mechanisms underlying changes in Glu levels and Glu metabolism, and their role in the RTT brain.

In conclusion, MeCP2 modulates Glu clearance through the regulation of astroglial genes in astrocytes. This study suggests a novel role for MeCP2 in astrocyte function; these findings may be useful in exploration of a new approach for preventing the neurological dysfunctions associated with RTT.

Materials and Methods

Cell culture

For each experiment, primary cultures were generated from individual MeCP2-null neonates and their wild-type littermates; tail snips from each neonate were obtained for genotyping, as described below. Enriched cultures of GFAP-expressing astroglial cells, which are virtually free of neurons and microglial cells, were established from the cerebral hemispheres of postnatal day (P) 0 to P1 newborn mice, as previously described [29]. In brief, pieces of dissected tissue were trypsinized (0.05%) for 10 min in Ca_2^+- and Mg_2^+-free phosphate-buffered saline (PBS) supplemented with

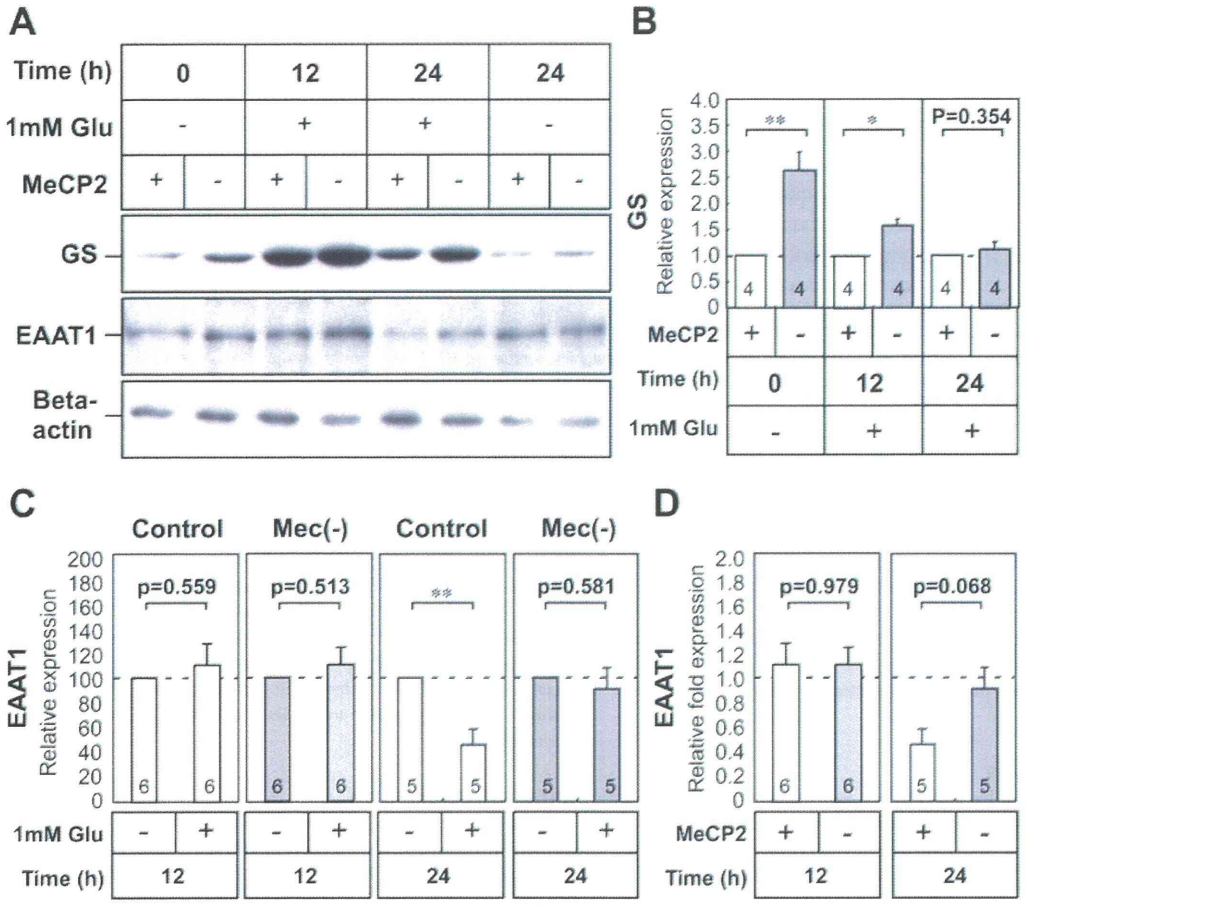

Figure 5. Effect of glutamate on glutamine synthetase and EAAT1 protein expression in MeCP2-null astrocytes. A. Time-dependent expression of GS and EAAT1 proteins in wild-type and MeCP2-deficient astrocyte cultures. Astrocytes were treated with 1.0 mM Glu for 24 h, and subsequently analyzed for expression of GS and EAAT1 by Western blot analysis. Beta-actin protein levels were analyzed in the same way, as an internal control. **B.** The immunoreactive GS protein bands were quantified by densitometry, normalized against β-actin levels, and expressed as fold change relative to the controls (equals 1.0). Bars represent the means ± SE of samples from three independent experiments (*$p<0.05$, **$p<0.01$). Numbers in each column indicate the total number of samples analyzed. **C.** The immunoreactive EAAT1 protein bands were quantified by densitometry, normalized against β-actin levels, and expressed as % of controls (equals 100%). Bars represent the means ± SE of samples from three independent experiments (**$p<0.01$). **D.** Comparison of the effects of Glu on EAAT1 expression in wild-type and MeCP2-null astrocytes. The ratio of EAAT1/β-actin in each treatment group was normalized against that of the non-treated astrocytes from each group. Bars represent the means ± SE of samples from three independent experiments. Numbers in each column indicate the total number of samples analyzed.
doi:10.1371/journal.pone.0035354.g005

0.02% EDTA. Tissue samples were subsequently dissociated in Hank's balanced salt solution (HBSS) containing 15% fetal calf serum (FCS; F2442, Sigma-Aldrich, Inc., St. Louis, MO, USA) by trituration though 10-ml plastic pipettes. Cells were pelleted at 100×g for 5 min, resuspended in Dulbecco's modified Eagle's medium (D-MEM; Wako Pure Chemical Industries, Ltd., Osaka, Japan) containing 15% FCS, and seeded into 100-mm culture dishes previously coated with poly-D-lysine (0.1 mg/ml; Wako Pure Chemical Industries, Ltd., Osaka, Japan). Upon reaching confluency, cells were trypsinized and replated. Cells were used after the third passage (P3) in all experiments, and were seeded at 3×10^4 cells/cm^2 in 6-well plate dishes or 35-mm culture dishes. Cultures were assayed by immunochemical analysis using antibodies against GFAP, MAP2, and CD11b in order to determine the degree of enrichment; the astrocyte cultures were nearly pure without contamination of microglia and neurons (Fig. S3 and Information S1).

Cell growth and bromo-2′-deoxyuridine (BrdU) uptake assay

To determine growth rate, cells were plated at 2×10^5 cells/dish in 35-mm dishes. At each passage, three dishes per cell line were harvested by trypsinization, and cell numbers were determined using a hemocytometer. Growth rate was expressed as the number of harvested cells divided by the number of seeded cells.

BrdU incorporation during DNA synthesis was determined using the 5-Bromo-2′-deoxy-uridine Labeling and Detection Kit I (Roche, Indianapolis, IN, USA). Briefly, cells were seeded at 3.0×10^4 cells per well in 48-well culture plates and incubated in D-MEM containing 10% FCS at 37°C for 24 h. After cells were

Table 1. PCR primers.

	Sense	Antisense	Ta	cycles
GFAP	5′-ATCCGCTCAGGTCATCTTACCC-3′	5′-TGTCTGCTCAATGTCTTCCCTACC-3′	63	25
S100β	5′-AGAGGACTCCAGCAGCAAAGG-3′	5′-AGAGAGCTCAGCTCCTTCGAG-3′	59	32
EAAT1	5′-GAAGTCTCCCAGACGTTCTAATCC-3′	5′-GCTCTGAAACCGCCACTTACTATC-3′	65	35
EAAT2	5′-ATGCTCATCCTCCCTCTTATCATC-3′	5′-CTTTCTTTGTCACTGTCTGAATCTG-3′	63	32
GS	5′-TGTACCTCCATCCTGTTGCC-3′	5′-GTCCCCGTAATCTTGACTCC-3′	57	25
HPRT	5′-CCTGCTGGATTACATTAAAGCACTG-3′	5′-AAGGGCATATCCAACAACAA-3′	57	30
MeCP2	5′-GGTAAAACCCGTCCGGAAAATG-3′	5′-TTCAGTGGCTTGTCTCTGAG-3′	61	35

GFAP, glial fibrillary acidic protein; EAAT, excitatory amino acid transporter; GS, glutamine synthetase; HPRT, hypoxantine-phosphoribosyl-transferase; MeCP2, methyl-CpG-binding protein 2; Ta, annealing temperature (°C).

doi:10.1371/journal.pone.0035354.t001

incubated with 10 μM BrdU for 2 h, they were fixed with 70% ethanol in 50 mM glycine (pH 2.0) for 20 min at −20°C. Cells were incubated with an anti-BrdU monoclonal antibody, followed by a fluorescein-coupled goat anti-mouse Ig and Hoechst33324 (1 μg/ml). To determine the percentages of BrdU-positive cells, fluorescent images were obtained by a Biorevo BZ-9000 fluorescence microscope (KEYENCE Co., Osaka, Japan); images were analyzed using the BZ-II application. BrdU-positive cells and total cells were counted in random 3 fields per well (approximately 1200 cells per well). Results were obtained from four independent experiments.

Cell Viability Analysis

Cell were seeded at 1×10^4 cells per well in 96-well plates and incubated in D-MEM containing 15% FCS at 37°C for 24 h. In injury models of drug and oxidative stress, cells were incubated with 0.01–10 mM glutamate for 24 h, 12.5–200 mM NH_4Cl (Sigma Chemical Co.) for 4 h, or 0.125–1.0 mM H_2O_2 (Wako Pure Chemical Industry, Osaka, Japan) for 1 h as previously described [28,39,40]. After 24 h of drug treatment, cell viability was determined using the WST-8 assay (NACALAI TESQUE, INC., Kyoto, Japan) [39,41].

PCR analysis

MeCP2$^{-/+}$ female mice (B6.129P2(C)-Mecp2$^{tm1.1Bird}$/J strain) were purchased from the Jackson Laboratory (Bar Harbor, ME) and mated with wild-type C57BL/6 male mice. DNA samples were extracted from tail snips from newborn animals; prior to nucleic acid extraction, snips were digested with proteinase K. Genotyping was performed by PCR analysis of genomic DNA according to the protocol provided by the manufacturer (http://jaxmice.jax.org/pub-cgi/protocols/protocols.sh?objtype=protocol&protocol_id=598) [4,12]. All experiments were performed in accordance with the National Institutes of Health Guidelines for the Care and Use of Laboratory Animals, and were approved by the Animal Research Committee of Kurume University.

Total RNA was extracted from cells using a Sepazol RNA I super kit (Nacalai Tesque, Inc., Kyoto, Japan) [41,42]. One microgram of total RNA was reverse transcribed, and 1/100 of the cDNA (equivalent to 10 ng of total RNA) was subjected to PCR amplification with Taq DNA polymerase (Promega, Co., Ltd., Madison, WI) using the following conditions: 25–35 cycles of 94°C for 30 s, annealing temperature for 60 s, and 74°C for 60 s. Primer sets and annealing temperatures are shown in Table 1. The most appropriate PCR conditions for semi-quantitative analysis of each gene were carefully determined by several preliminary experiments (Fig. S4). The number of cycles for GFAP, S100β, EAAT1, EAAT2, and GS was 25, 32, 35, 32, and 25, respectively (Table 1). The amplified cDNA was electrophoresed on 2% agarose gels containing ethidium bromide, and quantities were analyzed by densitometry using ImageJ software (the Research Service Branch of the National Institute of Health, Bethesda, MD, USA) [42]. The relative expression of each gene was normalized to the intensity of a housekeeping gene, hypoxantine-phosphoribosyl-transferase (HPRT; 30 cycles). The expression level of each gene is reported as a ratio relative to the level of normalized expression in a control sample.

Immunocytochemistry

Cultures were fixed with 4% paraformaldehyde for 10 min and permeabilized with 0.05% Triton-X 100 for 5 min. After blocking of nonspecific binding sites with 10% nonfat dry milk in PBS for 1 h, cultures were immunocytochemically stained using antibodies against MeCP2 (anti-MeCP2 polyclonal antibody, MILLIPORE, Temecula, CA, USA; anti-MeCP2 monoclonal antibody, G-6, Santa Cruz Biotechnology, Inc., Santa Cruz, CA), β-tubulin type III (TuJ, Sigma-Aldrich, Inc., St. Louis, Missouri), or glial fibrillary acidic protein (GFAP) (anti-GFAP polyclonal antibody, G9269; anti-GFAP monoclonal antibody, G3893, Sigma-Aldrich, Inc., St. Louis, Missouri), followed by secondary fluorescent antibodies as described previously [12]. Cultures were additionally stained with Hoechst33342 and examined using an Olympus IX-70 (Olympus Japan Inc. Tokyo, Japan) microscope. Photomicrographs were captured using an Olympus DP70 digital camera.

Immunoblotting

Cell extracts were prepared from astroglial cultures as described previously [41]. Western blot analysis was performed using anti-glutamine synthetase (G2781; Sigma-Aldrich, Inc., St. Louis, Missouri), anti-excitatory amino acid transporter 1 (EAAT1, GLAST; Santa Cruz Biotechnology, Inc., Santa Cruz, CA), horseradish peroxidase-conjugated anti-rabbit IgG (DakoCytomation, Glostrup, Denmark), and chemiluminescent substrate (Chemi-Lumi One, NACALAI TESQUE, INC., Kyoto, Japan) [12,41]. Several different exposure times were used for each blot to ensure linearity of band intensities. Immunoreactive bands were quantified using the ImageJ software (Research Service Branch of the National Institute of Health, Bethesda, MD, USA). The relative expression of each protein was normalized to the intensity of β-actin. The expression level of each protein is reported as a

ratio relative to the level of normalized expression in a control sample.

Glutamate Clearance Assay

To measure extracellular glutamate (Glu) concentrations, we used the Glutamate Assay Kit colorimetric assay (Yamasa Corporation, Tokyo, Japan) [43]. Assays were carried out in six independent trials. The clearance ratio of Glu was calculated from the Glu concentration (μM) in the medium sample of the drug-treated astroglial cells (Glu_{drug}) and the control non-drug treated (i.e., treated with drug vehicle alone) glial cells (Glu_{sol}). This is represented mathematically as follows: Glu clearance ratio = $(100-Glu_{drug})/(100-Glu_{solv})$. Threo-beta-benzyloxyaspartate (TBOA), UCPH-101 (2-amino-4-(4-methoxyphenyl)-7-(naphthalen-1-yl)-5-oxo-5,6,7,8-tetrahydro-4H-chromene-3-carbonitrile), or dihydrokainate (DHKA) (all purchased from Tocris Bioscience Ellisville, MO, USA) were applied to astroglial cells 60 min before Glu.

Statistical analysis

Quantitative results are expressed as means ± standard errors (SE). Student's t-test was used to compare data, with $p<0.05$ considered significant.

Supporting Information

Figure S1 BrdU-incorporating cells in wild-type and MeCP2-null astrocytes. The top and bottom pictures show BrdU-incorporating (Green) and Hoechst-stained (Blue) cells, respectively, which were stained with the primary anti-BrdU antibodies, the secondary fluorescein-coupled antibodies, and Hoechst 33324. Negative controls received identical treatments, but were not exposed to BrdU. Representative pictures were used to accurately count the number of BrdU incorporated cells to assess the efficiency of astrocyte cell growth. Scale bar = 200 μm.
(EPS)

Figure S2 Concentration dependency of GS and EAAT1 expression in wild-type and MeCP2-null astrocytes treated with Glutamate. The astrocytes of each group were treated with 0.01–1.0 mM Glu for 12 h, and subsequently analyzed for expression of GS and EAAT1 by western blot analysis.
(EPS)

Figure S3 Purity of astroglial cultures from mouse brain. The purity of astroglial cultures was assessed by immunocytochemisty (**A**) and immunoblotting (**B**) using antibodies against glial fibrillary acidic protein (GFAP; astrocyte marker; Sigma-Aldrich), CD11b (microglial marker; Santacruz), or microtubule associated protein 2 (MAP2; neuronal marker; Sigma-Aldrich). **A.** Immunocytochemistry indicates that neither CD11b nor MAP2 were expressed in astrocyte cultures. Positive control indicates microglia and mouse ES-derived neural cells that stained with anti-CD11b and MAP2 antibodies, respectively. Scale bar = 100 μm. **B.** Western blot analysis of protein extracts from cultured astrocytes and mouse whole brain. Western blot analysis also confirmed that the cultured astrocytes expressed GFAP, but did not express CD11b and MAP2.
(EPS)

Figure S4 Optimization of the semi-quantitative RT-PCR assay. Total RNA extracted from neonatal mouse brain astrocytes was serially diluted (2.5, 5, 10, 20, and 40 ng RNA in lanes 1, 2, 3, 4, and 5, respectively), reverse-transcribed and used as control samples in semi-quantitative RT-PCR for GFAP (**A**), S100β (**B**), HPRT (**C**), EAAT1 (**D**), EAAT2 (**E**), and GS (**F**). PCR was carried out for indicated cycles using each of primer sets shown in Table 1. The amplified cDNA was electrophoresed in a 2% agarose gel containing ethidium bromide. NT, RT-PCR with no template.
(EPS)

Information S1 Supporting materials and methods.
(DOC)

Author Contributions

Conceived and designed the experiments: YO TT. Performed the experiments: YO CM TT. Analyzed the data: YO TT ET. Contributed reagents/materials/analysis tools: KK TM. Wrote the paper: YO TT.

References

1. Chahrour M, Zoghbi HY (2007) The story of Rett syndrome: from clinic to neurobiology. Neuron 56: 422–437.
2. Matsuishi T, Yamashita Y, Takahashi T, Nagamitsu S (2011) Rett syndrome: The state of clinical and basic research, and future perspectives. Brain Dev 33: 623–631.
3. Amir RE, Van den Veyver IB, Wan M, Tran CQ, Francke U, et al. (1999) Rett syndrome is caused by mutations in X-linked MECP2, encoding methyl-CpG-binding protein 2. Nat Genet 23: 185–188.
4. Guy J, Hendrich B, Holmes M, Martin JE, Bird A (2001) A mouse Mecp2-null mutation causes neurological symptoms that mimic Rett syndrome. Nat Genet 27: 322–326.
5. Chen RZ, Akbarian S, Tudor M, Jaenisch R (2001) Deficiency of methyl-CpG binding protein-2 in CNS neurons results in a Rett-like phenotype in mice. Nat Genet 27: 327–331.
6. Calfa G, Percy AK, Pozzo-Miller L (2011) Experimental models of Rett syndrome based on Mecp2 dysfunction. Exp Biol Med (Maywood) 236: 3–19.
7. Bienvenu T, Chelly J (2006) Molecular genetics of Rett syndrome: when DNA methylation goes unrecognized. Nat Rev Genet 7: 415–426.
8. Saywell V, Viola A, Confort-Gouny S, Le Fur Y, Villard L, et al. (2006) Brain magnetic resonance study of Mecp2 deletion effects on anatomy and metabolism. Biochem Biophys Res Commun 340: 776–783.
9. Ballas N, Lioy DT, Grunseich C, Mandel G (2009) Non-cell autonomous influence of MeCP2-deficient glia on neuronal dendritic morphology. Nat Neurosci 12: 311–317.
10. Maezawa I, Swanberg S, Harvey D, LaSalle JM, Jin LW (2009) Rett syndrome astrocytes are abnormal and spread MeCP2 deficiency through gap junctions. J Neurosci 29: 5051–5061.
11. Maezawa I, Jin LW (2010) Rett syndrome microglia damage dendrites and synapses by the elevated release of glutamate. J Neurosci 30: 5346–5356.
12. Okabe Y, Kusaga A, Takahashi T, Mitsumasu C, Murai Y, et al. (2010) Neural development of methyl-CpG-binding protein 2 null embryonic stem cells: a system for studying Rett syndrome. Brain Res 1360: 17–27.
13. Lioy DT, Garg SK, Monaghan CE, Raber J, Foust KD, et al. (2011) A role for glia in the progression of Rett's syndrome. Nature 475: 497–500.
14. Seifert G, Schilling K, Steinhauser C (2006) Astrocyte dysfunction in neurological disorders: a molecular perspective. Nat Rev Neurosci 7: 194–206.
15. Eroglu C, Barres BA (2010) Regulation of synaptic connectivity by glia. Nature 468: 223–231.
16. Sheldon AL, Robinson MB (2007) The role of glutamate transporters in neurodegenerative diseases and potential opportunities for intervention. Neurochem Int 51: 333–355.
17. Eid T, Williamson A, Lee TS, Petroff OA, de Lanerolle NC (2008) Glutamate and astrocytes–key players in human mesial temporal lobe epilepsy? Epilepsia 49 Suppl 2: 42–52.
18. Hamberger A, Gillberg C, Palm A, Hagberg B (1992) Elevated CSF glutamate in Rett syndrome. Neuropediatrics 23: 212–213.
19. Lappalainen R, Riikonen RS (1996) High levels of cerebrospinal fluid glutamate in Rett syndrome. Pediatr Neurol 15: 213–216.
20. Pan JW, Lane JB, Hetherington H, Percy AK (1999) Rett syndrome: 1H spectroscopic imaging at 4.1 Tesla. J Child Neurol 14: 524–528.
21. Horska A, Farage L, Bibat G, Nagae LM, Kaufmann WE, et al. (2009) Brain metabolism in Rett syndrome: age, clinical, and genotype correlations. Ann Neurol 65: 90–97.
22. Ward BC, Kolodny NH, Nag N, Berger-Sweeney JE (2009) Neurochemical changes in a mouse model of Rett syndrome: changes over time and in response to perinatal choline nutritional supplementation. J Neurochem 108: 361–371.

23. Viola A, Saywell V, Villard L, Cozzone PJ, Lutz NW (2007) Metabolic fingerprints of altered brain growth, osmoregulation and neurotransmission in a Rett syndrome model. PLoS One 2: e157.
24. Dunn HG, MacLeod PM (2001) Rett syndrome: review of biological abnormalities. Can J Neurol Sci 28: 16–29.
25. Naidu S, Kaufmann WE, Abrams MT, Pearlson GD, Lanham DC, et al. (2001) *Neuroimaging studies in Rett syndrome*. Brain Dev 23 Suppl 1: S62–71.
26. Colantuoni C, Jeon OH, Hyder K, Chenchik A, Khimani AH, et al. (2001) Gene expression profiling in postmortem Rett Syndrome brain: differential gene expression and patient classification. Neurobiol Dis 8: 847–865.
27. Setoguchi H, Namihira M, Kohyama J, Asano H, Sanosaka T, et al. (2006) Methyl-CpG binding proteins are involved in restricting differentiation plasticity in neurons. J Neurosci Res 84: 969–979.
28. Chen CJ, Liao SL, Kuo JS (2000) Gliotoxic action of glutamate on cultured astrocytes. J Neurochem 75: 1557–1565.
29. Lehmann C, Bette S, Engele J (2009) High extracellular glutamate modulates expression of glutamate transporters and glutamine synthetase in cultured astrocytes. Brain Res 1297: 1–8.
30. Shigeri Y, Seal RP, Shimamoto K (2004) Molecular pharmacology of glutamate transporters, EAATs and VGLUTs. Brain Res Brain Res Rev 45: 250–265.
31. Erichsen MN, Huynh TH, Abrahamsen B, Bastlund JF, Bundgaard C, et al. (2010) Structure-activity relationship study of first selective inhibitor of excitatory amino acid transporter subtype 1: 2-Amino-4-(4-methoxyphenyl)-7-(naphthalen-1-yl)-5-oxo-5,6,7,8-tetrahydro-4 H-chromene-3-carbonitrile (UCPH-101). J Med Chem 53: 7180–7191.
32. Deguchi K, Antalffy BA, Twohill LJ, Chakraborty S, Glaze DG, et al. (2000) Substance P immunoreactivity in Rett syndrome. Pediatr Neurol 22: 259–266.
33. Namihira M, Nakashima K, Taga T (2004) Developmental stage dependent regulation of DNA methylation and chromatin modification in a immature astrocyte specific gene promoter. FEBS Lett 572: 184–188.
34. Tsujimura K, Abematsu M, Kohyama J, Namihira M, Nakashima K (2009) Neuronal differentiation of neural precursor cells is promoted by the methyl-CpG-binding protein MeCP2. Exp Neurol 219: 104–111.
35. Jellinger K, Armstrong D, Zoghbi HY, Percy AK (1988) Neuropathology of Rett syndrome. Acta Neuropathol 76: 142–158.
36. Kim SY, Choi SY, Chao W, Volsky DJ (2003) Transcriptional regulation of human excitatory amino acid transporter 1 (EAAT1): cloning of the EAAT1 promoter and characterization of its basal and inducible activity in human astrocytes. J Neurochem 87: 1485–1498.
37. Yang Y, Gozen O, Vidensky S, Robinson MB, Rothstein JD (2010) Epigenetic regulation of neuron-dependent induction of astroglial synaptic protein GLT1. Glia 58: 277–286.
38. Ricciardi S, Boggio EM, Grosso S, Lonetti G, Forlani G, et al. (2011) Reduced AKT/mTOR signaling and protein synthesis dysregulation in a Rett syndrome animal model. Hum Mol Genet 20: 1182–1196.
39. Ushikoshi H, Takahashi T, Chen X, Khai NC, Esaki M, et al. (2005) Local overexpression of HB-EGF exacerbates remodeling following myocardial infarction by activating noncardiomyocytes. Lab Invest 85: 862–873.
40. Norenberg MD, Jayakumar AR, Rama Rao KV, Panickar KS (2007) New concepts in the mechanism of ammonia-induced astrocyte swelling. Metab Brain Dis 22: 219–234.
41. Takahashi T, Kawai T, Ushikoshi H, Nagano S, Oshika H, et al. (2006) Identification and isolation of embryonic stem cell-derived target cells by adenoviral conditional targeting. Mol Ther 14: 673–683.
42. Kawai T, Takahashi T, Esaki M, Ushikoshi H, Nagano S, et al. (2004) Efficient cardiomyogenic differentiation of embryonic stem cell by fibroblast growth factor 2 and bone morphogenetic protein 2. Circ J 68: 691–702.
43. Takeuchi H, Mizuno T, Zhang G, Wang J, Kawanokuchi J, et al. (2005) Neuritic beading induced by activated microglia is an early feature of neuronal dysfunction toward neuronal death by inhibition of mitochondrial respiration and axonal transport. J Biol Chem 280: 10444–10454.

nature COMMUNICATIONS

OPEN

ARTICLE

Received 21 Oct 2011 | Accepted 20 Feb 2012 | Published 27 Mar 2012

DOI: 10.1038/ncomms1755

FAD-dependent lysine-specific demethylase-1 regulates cellular energy expenditure

Shinjiro Hino[1], Akihisa Sakamoto[1], Katsuya Nagaoka[1], Kotaro Anan[1], Yuqing Wang[2], Shinya Mimasu[3,4], Takashi Umehara[3], Shigeyuki Yokoyama[3,4], Ken-ichiro Kosai[2] & Mitsuyoshi Nakao[1,5]

Environmental factors such as nutritional state may act on the epigenome that consequently contributes to the metabolic adaptation of cells and the organisms. The lysine-specific demethylase-1 (LSD1) is a unique nuclear protein that utilizes flavin adenosine dinucleotide (FAD) as a cofactor. Here we show that LSD1 epigenetically regulates energy-expenditure genes in adipocytes depending on the cellular FAD availability. We find that the loss of LSD1 function, either by short interfering RNA or by selective inhibitors in adipocytes, induces a number of regulators of energy expenditure and mitochondrial metabolism such as PPARγ coactivator-1α resulting in the activation of mitochondrial respiration. In the adipose tissues from mice on a high-fat diet, expression of LSD1-target genes is reduced, compared with that in tissues from mice on a normal diet, which can be reverted by suppressing LSD1 function. Our data suggest a novel mechanism where LSD1 regulates cellular energy balance through coupling with cellular FAD biosynthesis.

[1] Department of Medical Cell Biology, Institute of Molecular Embryology and Genetics, the Global Center of Excellence 'Cell Fate Regulation Research and Education Unit', Kumamoto University, 860-0811, Japan. [2] Department of Gene Therapy and Regenerative Medicine, Advanced Therapeutics Course, Graduate School of Medical and Dental Sciences, Kagoshima University, 890-8544, Japan. [3] RIKEN Systems and Structural Biology Center, Yokohama 230-0045, Japan. [4] Graduate School of Science, The University of Tokyo, 113-0033, Japan. [5] Core Research for Evolutional Science and Technology (CREST), Japan Science of Technology Agency, Tokyo, Japan. Correspondence and requests for materials should be addressed to S.H. (email: s-hino@kumamoto-u.ac.jp) or to M.N. (email: mnakao@gpo.kumamoto-u.ac.jp).

In response to environmental stimuli, epigenetic marks such as DNA and histone methylation may be dynamically added and removed for gene regulation during the transcriptional cycle[1,2]. Nutritional information may influence the epigenome by directly affecting the activities of epigenetic modifiers[3]. Notably, it has been reported that nutritional conditions in early life influence the susceptibility to chronic disorders, such as obesity and related metabolic diseases, later in life[4], suggesting underlying epigenetic mechanisms[5]. Thus, elucidating how nutritional information is transferred to the epigenetic machinery for the regulation of cellular metabolism, and the formation of the long-term metabolic phenotype is of great interest.

Lysine-specific demethylase-1 (LSD1, also known as KDM1A) is a member of the flavin-containing amine oxidase family that, in general, represses transcription by removing the methyl group from mono-methylated and di-methylated lysine 4 of histone H3 (H3K4)[6]. LSD1 is also involved in the demethylation of H3K9 when associated with some nuclear receptors[7], and in the demethylation of non-histone proteins such as p53, Stat3 and Dnmt1 (ref. 8–10), suggesting its contribution to selective biological processes. Indeed, genetic ablation of LSD1 in mice causes embryonic lethality[11], and LSD1-deficient embryonic stem cells had cell defects and global DNA hypomethylation[10], consistent with the important functions of LSD1.

Among numerous epigenetic factors, LSD1 is unique in that it utilizes flavin adenosine dinucleotide (FAD) as an essential cofactor for catalytic activities[12]. FAD serves as a coenzyme in many oxidative reactions including mitochondrial fatty acid β-oxidation and in the respiratory chain[13]. The majority of reported flavoenzymes localize to the mitochondria or cytoplasm, whereas LSD1 is one of a few flavoproteins in the nucleus. Another nuclear flavoprotein is apoptosis-inducing factor (AIF) that initially localizes to the mitochondrial inner membrane and translocates to the nucleus on oxidative stress or other proapoptotic stimuli, leading to DNA degradation[14], suggesting that AIF may transfer the mitochondrial metabolic information to the nucleus[15]. However, the biological significance of FAD-dependent LSD1 activities in metabolic regulation remains unknown.

In this study, we present direct evidence that the inhibition of LSD1, by short interfering RNA (siRNA)-mediated knockdown (KD) and by selective inhibitors, activates energy-expenditure genes by transcriptional and epigenetic mechanisms in adipocytes. Disruption of LSD1 function resulted in the de-repression of these genes leading to the activation of mitochondrial respiration and lipolysis in adipocytes. We further found that LSD1-mediated transcriptional repression is FAD-dependent, and that the disruption of cellular FAD synthesis exerted similar effects on the metabolic gene expression as the LSD1 inhibition. Importantly, the expression of LSD1-target genes was markedly repressed in high fat-exposed white adipose tissue (WAT), and could be reverted by LSD1 inhibition, indicating the involvement of LSD1 in metabolic adaptation *in vivo*. Our data shed light on an essential mechanism of energy utilization that might explain how cells determine their energy strategy depending on nutritional availability.

Results

LSD1 regulates energy-expenditure genes in adipocytes. During our investigations, we found that both LSD1 and its essential partner BHC80 (ref. 16), showed relatively high expression levels in WAT among metabolic tissues in mice (Fig. 1a; Supplementary Fig. S1a). In addition, adipogenic 3T3-L1 cells abundantly expressed BHC80, which was found to form a complex with LSD1 in these cells (Fig. 1b; Supplementary Fig. S1b,c). During adipogenesis, an increase in mono-methylated H3K4 was observed, which is indicative of the active regulation of H3K4 methylation in these cells (Supplementary Fig. S1d). To address the role of LSD1 function in adipose cells, we performed microarray-based expression analyses in 3T3-L1 cells. We disrupted LSD1 function by using specific siRNAs for LSD1 and BHC80 (Fig. 1c), as well as by using an LSD1 inhibitor, tranylcypromine (TC, also known as trans-2-phenylcyclopropylamine)[17–21], in adipocyte-differentiating 3T3-L1 cells. TC was initially identified as an inhibitor of monoamine oxidases (MAO) A and B[22], and was demonstrated to be a potent inhibitor of LSD1 (refs 17,18). In agreement with the transcriptional repressive activities of LSD1, 198 probe sets were commonly induced 1.5-fold or more by LSD1-KD, BHC80-KD and TC treatment (Fig. 1d; Supplementary Data 1). Focusing on the probe sets upregulated by LSD1-KD, we found significant enrichment of the probe sets that were similarly upregulated by TC ($P=2.8\times10^{-56}$ by χ^2 test), while only a few were oppositely regulated (Fig. 1e). A similar tendency was observed for the co-target probes of LSD1-KD and BHC80-KD ($P=8.0\times10^{-8}$ by χ^2 test). To clarify the biological relevance of the co-target genes, we used Gene set enrichment analysis[23] (Fig. 1f). Considering the physiological function of adipocytes, we found that many of the co-target genes were related to lipid metabolism and mitochondrial oxidative phosphorylation (OXPHOS). On the other hand, 95 probe sets were commonly downregulated more than 1.5-fold by LSD1-KD, BHC80-KD and TC. However, GSEA analysis of the downregulated genes under LSD1 inhibition identified no significantly enriched gene sets associated with energy metabolism (Fig. 1g; Supplementary Data 2).

By quantitative RT–PCR analyses, we confirmed that important regulators of energy metabolism (Fig. 2a), such as PPARγ coactivator-1α (PGC-1α), pyruvate dehydrogenase kinase 4 (PDK4), protein kinase A regulatory subunit 2 alpha (RIIalpha) and adipose triglyceride lipase (ATGL), were significantly upregulated (Fig. 2b,c; Supplementary Data 1). These gene products have been reported to have key roles in mitochondrial energy production and/or lipid mobilization[24–27]. Among them, elevated expression of PGC-1α is a hallmark of brown adipose tissue (BAT), which is specialized for consumptive metabolism for the purpose of thermogenesis[28]. Consistently, LSD1 inhibition induced the expression of fatty acid transporter 1 (FATP1), a critical regulator of BAT metabolism (Fig. 2b,c)[29,30]. The selective upregulation of the group of energy-expenditure genes was confirmed by the use of alternative siRNA against LSD1 (Fig. 2d,e). We also noticed that LSD1 inhibition did not affect the expression of the key adipogenic factors as well as the drivers of brown adipogenesis (Supplementary Table S1).

As TC is also a potent MAO inhibitor, we employed selective LSD1 inhibitors (SLIs) to discriminate whether the activation of the metabolic genes is attributable to specific inactivation of the enzymatic activity of LSD1. We used three SLIs, S2101, S2107 and S2111, which are structurally related to TC, but highly potent with substantially reduced affinity to MAOs (Supplementary Fig. S2a)[31]. All SLIs showed coherent effects against LSD1-target metabolic genes, suggesting a strong link between the enzymatic activity of LSD1 and energy metabolism (Fig. 2c). In addition, MAO inhibitors, pargyline and clorgyline[17], did not activate LSD1-target genes at the tested concentrations (Supplementary Fig. S2b). Consistently, IC50 values of LSD1 and MAO inhibitors correlate well with the activation of LSD1-target genes by these drugs (Supplementary Table S2). The expression microarray analysis, using the cells treated with SLIs, confirmed the selectivity of these drugs, and further emphasized the link between LSD1 enzymatic activity and metabolic gene regulation (Supplementary Fig. S2c,d). Collectively, these results indicate that LSD1 represses expression of the energy-expenditure genes in adipocytes.

LSD1 epigenetically represses energy-expenditure genes. To investigate the molecular mechanism of LSD1 action, we tested whether energy-expenditure genes are directly regulated by LSD1 in differentiating 3T3-L1 cells. Chromatin immunoprecipitation (ChIP) analysis revealed that LSD1 was specifically enriched near

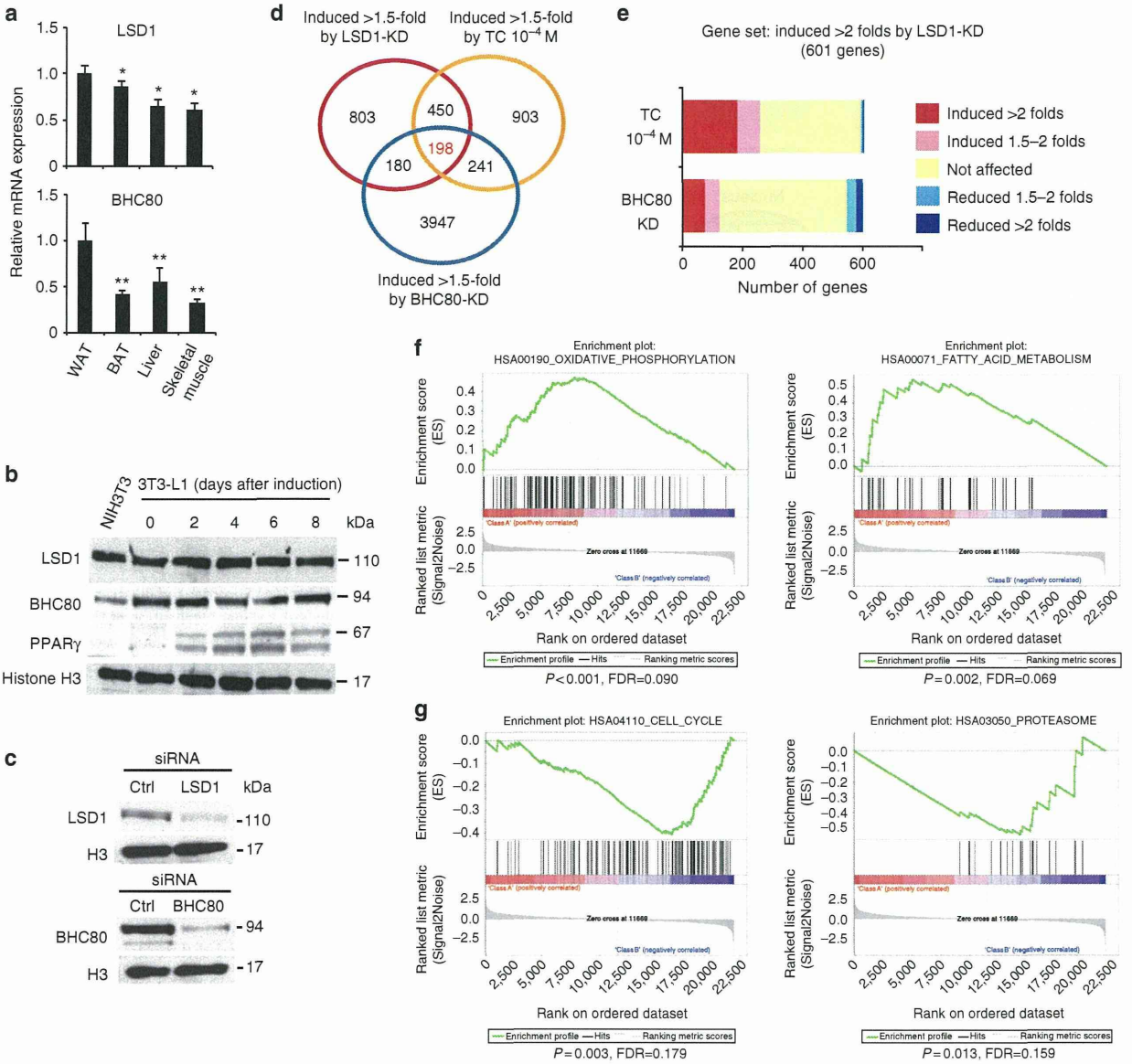

Figure 1 | Genome-wide analyses of LSD1-regulated genes in adipocytes. (**a**) Preferential expression of LSD1 and BHC80 in WAT. Expression of *LSD1* and *BHC80* mRNAs in epididymal WAT, interscapular BAT, liver and skeletal muscle. 13-week old C57BL/6J mice were fasted for 16 h before tissue dissection. Quantitative RT-PCR values were normalized to the expression levels of the housekeeping *36B4* gene, and are shown as means±s.d. of four mice. $^{*}P<0.05$, $^{**}P<0.01$ versus WAT by Student's *t*-test. (**b**) The protein expression of LSD1 and BHC80 in adipogenic 3T3-L1 cells. The cells were subjected to adipogenic induction as described in Methods, and were collected at the indicated time points. (**c**) Specific siRNA-mediated knockdown of LSD1 and BHC80 in 3T3-L1 cells. *In silico* analysis, using mouse genome and EST databases, confirmed the target specificities of the siRNAs. For western blot analysis, protein samples were prepared 72 h after siRNA introduction. (**d**) Venn diagram of the genes induced 1.5-fold or more by LSD1-knockdown (KD), BHC80-KD or TC treatment. siRNA-introduced or TC-treated 3T3-L1 cells were subjected to adipogenic induction for 24 h. Control siRNA or vehicle-treated samples were used as controls. (**e**) Unidirectional effects of TC and BHC80-KD on LSD1-target genes. (**f**) Gene set enrichment analysis of commonly upregulated genes by LSD1-KD, BHC80-KD and TC treatment. In each panel, nominal *P*-values and false discovery rates (FDRs) are indicated. (**g**) Gene set enrichment analysis of commonly downregulated genes by LSD1-KD, BHC80-KD and TC treatment. Significantly enriched gene sets are shown. Nominal *P*-values and FDRs are indicated.

the transcription start site of the *PGC-1α* promoter (sites 3 and 4) (Fig. 3a). Similarly, the selective occupancy of LSD1 was observed at the *PDK4*, *FATP1* and *ATGL* gene promoters but not at the *actB* gene promoter (encoding β-actin) (Fig. 3b). The enrichment of di/tri-methylated H3K4 as well as acetylated H3 was enhanced by LSD1-KD at LSD1-bound promoters, whereas the *actB* promoter remained unchanged (Fig. 3c,d). Moreover, *Pdx1* gene, which is not expressed in adipose cells, showed enriched LSD1 occupancy and the increased H3K4 methylation after LSD1-KD, emphasizing the close relationship between LSD1 and H3K4 demethylation in energy-expenditure genes (Fig. 3b,c). Di-methylated H3K4 was enriched at the *PGC-1α* promoter under the TC treatment (Fig. 3e), consistent with the inhibition of LSD1-dependent demethylation by TC.

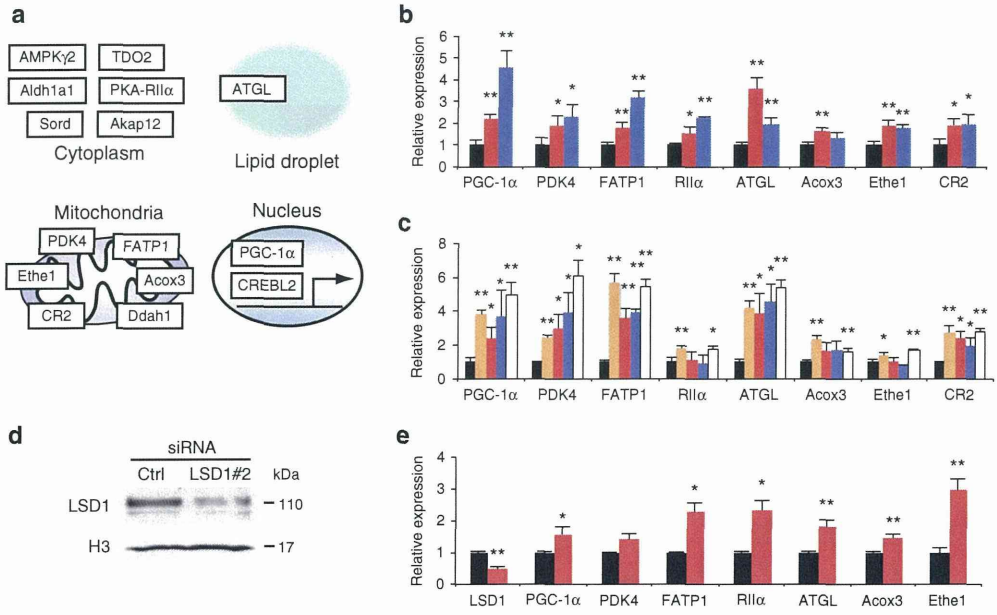

Figure 2 | LSD1 inhibition activates genes for energy expenditure and mitochondrial metabolism in adipocytes. (**a**) Summarized illustration of co-target genes. Co-target genes , associated with energy expenditure and mitochondrial metabolism, are shown with cellular localization of the gene products. (**b**) Expression levels of LSD1 target genes under LSD1-KD (red bars) and BHC80-KD (blue bars). Quantitative RT-PCR values were normalized to the expression levels of the *36B4* gene, and are shown as the fold difference against control siRNA-introduced samples (black bars). (**c**) Expression levels of LSD1 target genes after TC (orange bars) or SLIs (S2101 (red bars), S2107 (blue bars), S2111 (white bars)) treatment. TC and SLIs were used at the concentrations of 10^{-4} M and 10^{-5} M, respectively. Values are shown as the fold difference against vehicle-treated samples (black bars). (**d**) The knockdown of LSD1 using an alternative siRNA (LSD1#2). (**e**) The effect of LSD1 siRNA#2 on the expression of newly identified LSD1-target genes. Values are shown as the fold difference against control siRNA-introduced samples (black bars). All histogram data are means±s.d. of triplicate results. $^{*}P<0.05$, $^{**}P<0.01$ versus control by Student's *t*-test.

We then investigated the mechanism of LSD1-mediated transcriptional repression. LSD1-regulated promoters were enriched with relatively high levels of methylated H3K4, consistent with their active transcription in adipose cells (Fig. 3f). The knockdown of H3K4 methyltransferase Set7/9 resulted in a partial reduction of methylated H3K4, suggesting that methylation equilibrium on these promoters was formed through active methylation/demethylation forces (Fig. 3g). Treatment of the cells with Trichostatin A (TSA), a HDAC inhibitor, induced histone H3 acetylation of the energy-expenditure genes without affecting H3K4 methylation status (Fig. 3h). This suggests that enhanced H3K4 methylation by LSD1 inhibition was not merely a reflection of active chromatin formation, but rather indicates the direct relationship between LSD1 function and H3K4 methylation on these promoters. Typical repressive histone marks, methylated H3K9 and H3K27, were detected only at background levels on LSD1-target promoters, and were not influenced by LSD1-KD (Fig. 3i).

To assess promoter silencing by LSD1, reporter assays were performed in which the mouse *PGC-1α* promoter was fused to the *luciferase* reporter gene (PGC-1α/Luc) (Fig. 4a). As expected, PGC-1α/Luc activity was induced by LSD1-KD and BHC80-KD (Fig. 4b). As well, TC and SLIs significantly activated the *PGC-1α* promoter (Fig. 4c,d). We also examined the chromatin regulation of the PGC-1α/Luc transgene by LSD1. The ChIP assay confirmed that the transfected PGC-1α/Luc plasmid was engaged with histone H3, indicating the incorporation of the transgene into the nucleosome structure (Fig. 4e). TC treatment induced the increase of H3K4 di-methylation at the 5′ region of the transgenic PGC-1α promoter where LSD1 was bound (Fig. 4f,g). Thus, energy-expenditure genes are direct targets of the LSD1-mediated repression.

LSD1 inhibition activates mitochondrial metabolism. As the LSD1 inhibition resulted in the expression of energy-expenditure genes associated with mitochondrial metabolism, we sought to determine the metabolic consequences of LSD1-inhibited conditions. To address this, LSD1-inhibited differentiating 3T3-L1 cells were stained with JC-1, a fluorescent dye that binds to the mitochondrial inner membrane showing green fluorescence (FL1; mitochondrial mass) and forms red-fluorescent aggregates depending on the membrane potential (FL2; respiratory activity)[32]. Flow cytometric analyses of JC-1-stained cells revealed that LSD1-KD significantly augmented the mitochondrial membrane potential with an elevated FL2/FL1 ratio that represents the respiratory activity relative to the mitochondrial surface area (Fig. 5a). TC and SLIs also potently augmented the mitochondrial metabolism although pargyline did not (Fig. 5b; Supplementary Fig. 3a,b). The activated oxidative metabolism by LSD1 inhibition was also confirmed by measuring the OXPHOS capacity using a XF24 Extracellular Flux Analyzer (Seahorse). The maximum OXPHOS capacity was dramatically potentiated by LSD1-KD (Fig. 5c). On the other hand, glycolytic activity, as determined by cellular lactate production, was not significantly affected by either LSD1-KD or TC (Supplementary Fig. S3c,d).

To characterize the metabolic properties of mature adipocytes under *LSD1 inhibition*, we used an adenovirus-based method to introduce short hairpin RNA (shRNA) into mature 3T3-L1 adipocytes (Supplementary Fig. S4a). LSD1-KD resulted in the significant reduction of lipid accumulation only when the lipogenesis was enhanced under insulin-stimulated condition (Fig. 5d). Consistently, insulin-induced repression of energy-expenditure genes was attenuated by LSD1-KD (Supplementary Fig. 4b). In the insulin-stimulated adipocytes, oxidative metabolism was activated by LSD1-KD and TC treatment (Fig. 5e,f). LSD1 inhibition also reduced